The 2013 World Congress on
Advances in Structural Engineering and Mechanics (ASEM13)
Jeju, Korea, September 8-12, 2013

Residual bearing capacity of riveted steel ties deformed by the swelling of interstitial rust

*Pier Giorgio Malerba[1)] and Luca Sgambi[2)]

[1), 2)] *Dep. of Civil and Environmental Engineering, Politecnico di Milano, Milan, Italy*
[1)] piergiorgio.malerba@polimi.it

ABSTRACT

Old steel bridges were made of structural elements composed by riveted angles and sheets, placed side by side and without gaps among their surfaces. After decades of service such composed members exhibit dangerous distortions due to the rust grown inside the interstices and to its swelling over time.
Aim of this paper is to propose a model suitable to study the residual bearing capacity of riveted steel ties, deformed by the swelling of interstitial rust.

Keywords: old steel bridges; rust swelling; residual bearing capacity

1. INTRODUCTION

The structural reliability of old bridges still in service is a wide and common problem in the whole world. A typical case is that of steel bridges built at the beginning of the twentieth century, characterized by less resistant materials, built with very different technologies with respects to the current ones and designed for lower traffic loads (Malerba 2013).

Typical of that era was the use of structural elements composed by riveting elementary steel shapes (angles and sheets) placed side by side and without gaps among their surfaces. After decades of service, we are seeing dangerous distortions of such composed members, due to rust grown inside the interstices and to the swelling of this rust layer over time (Fig. 1).

Aim of this paper is to create a model which, on the basis of surveying data, should be able to describe the interaction between the rust swelling of a composite profile and the corresponding reduction in its bearing capacity.

2. PROBLEM DEFINITION

We consider a tied bar, composed by two rectangular rods having section $(b \times h)$ and

[1)] Professor
[2)] Assistant Professor

jointed by rivets placed at a given pitch L (Fig. 2). The rods are faced each other at contact, without gaps. Actually, small surface irregularities make the two rods not perfectly adherent and allow water and humidity to penetrate through preferential paths. This predisposition may be fostered by localized grinding, caused by the rivets clenching.

Fig. 1 Truss members deformed by rust swelling

Inside these small voids, interstitial layers of iron oxides start to form. As known, rust has a high expansion coefficient. It follows that once the phenomenon has started, it continues to grow, increasing the thickness of the layer of rust and deforming the rods. The rods open wide, constrained only by the rivets and assume permanent deformations. Gradually, the rods get to work in completely different way with respect to initial hypotheses, which consider them straight and simply stretched, and as a result they turn out to be overstressed with respect to the design assumptions.

This paper studies the residual bearing capacity of riveted steel ties deformed by the swelling of interstitial rust.

3. TIE MODELLING

Recent surveys on steel bridges built at the beginning of ‘900, showed how, along the segments between the rivets, such swelling phenomenon gives rise to regular and repeated lenticular diverging shapes, with opening of some millimeters at the middle. This suggested a simple model based on the following hypotheses

1. steel has linear elastic/perfectly plastic behaviour;
2. rivets elongation and section reduction, due to the corrosion, are ignored;
3. the tie is stretched by a tension force only;
4. the rods open wide because of the interstitial pressure distribution exerted by the rust lens grown between them;
5. the pressure profile is assumed affine to the deformed shape;
6. in the following we consider two deformed shapes: the first one (shape function A, Fig. 2(b)) according to a cosinusoidal function and the other (shape function B, Fig. 2(c)) according to a sinusoidal function. The first shape is more similar to the actual deformed profiles, with a maximum at the middle and no rotations at the riveted end sections. The other shape would take into account that the riveted sections may be weaker with respect to the current rod section and so we simply assume that the ends are free to rotate.

The model development starts with a short recall of the elastic behaviour of both cosinusoidal and sinusoidal shapes. Then, due to a load path which gradually increases the interstitial pressure, the elastic-plastic response is studied. For growing values of the axial force, the results give the evolution of the relative displacement at the middle of the tie segment and are summarized through (maximum pressure)/(relative displacement) diagrams.

4. ELASTIC BEHAVIOUR

Firstly we consider shape function A. The tie segment, having section $2\cdot(b\times h)$ and length L, is assumed as clamped at the end riveted sections and loaded by a force per unit of length $f(x)=p\cdot b$ given by the relationship (Fig. 2(b)):

$$f(x)=\frac{\overline{f}}{2}\cdot\left[1-\cos\left(\frac{2\cdot\pi\cdot x}{L}\right)\right] \tag{1}$$

where $\overline{f}$ is the maximum force intensity at the middle.

The force resultant F over the length L is:

$$F = \int_0^L \frac{\overline{f}}{2}\left[1-\cos\left(\frac{2\cdot\pi\cdot x}{L}\right)\right]\cdot dx = \frac{\overline{f}\cdot L}{2} \tag{2}$$

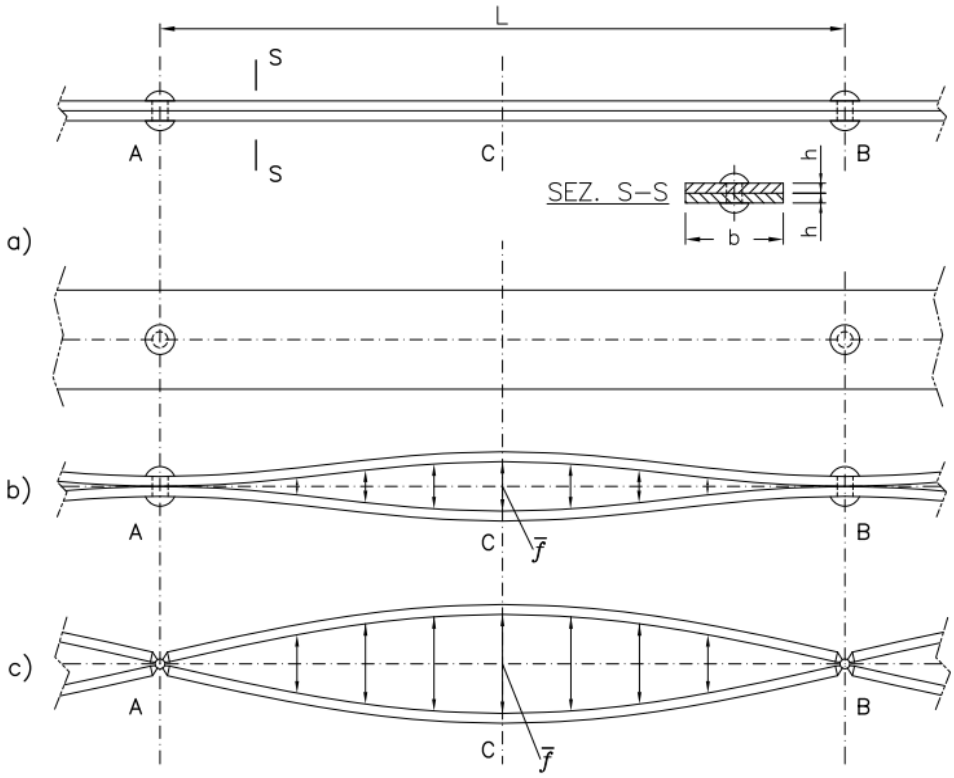

Fig. 2 Tied bar composed by two rectangular rods, riveted at a pitch L
(a) undeformed configuration; (b) deformed shape A (cosinusoidal) (c) deformed shape B (sinusoidal)

The elastic equilibrium equation is

$$E\cdot I\cdot\frac{dv^{IV}(x)}{dx^{IV}} = f\left(x\right) \tag{3}$$

Such an equation, integrated by taking into account the condition of clamped ends, leads to the following force - displacement relationship

$$v\left(x\right) = \frac{\overline{f}\cdot L^4}{E\cdot I}\cdot\left\{\frac{1}{48}\xi^4 - \frac{1}{32\cdot\pi^4}\cdot\left[\cos\left(\frac{2\cdot\pi\cdot x}{L}\right)\right] - \frac{1}{24}\cdot\xi^3 + \frac{1}{48}\cdot\xi^2 + \frac{1}{32\cdot\pi^4}\right\} \tag{4}$$

The corresponding bending moments at the ends A and B and at the middle C, are listed in Table 1.

Table 1 Bending moments at the ends and at the middle of the tie segment

	Section	Bending Moments
End sections	$x = 0;\ x = L$	$M_{Ap} = M_{Bp} = \overline{f} \cdot L^2 \cdot \left(\frac{3+\pi^2}{24 \cdot \pi^2} \right) = \frac{\overline{f} \cdot L^2}{\alpha} \cong \frac{\overline{f} \cdot L^2}{18.41}$
Middle section	$x = L/2$	$M_{Cp} = -\overline{f} \cdot L^2 \cdot \left(\frac{6+\pi^2}{48 \cdot \pi^2} \right) = -\frac{\overline{f} \cdot L^2}{\beta} \cong -\frac{\overline{f} \cdot L^2}{29.85}$

According to shape function B (Fig 2(c)), the tie segment is loaded by the sinusoidal force per unit of length

$$f(x) = \overline{f} \cdot \sin\left(\frac{\pi \cdot x}{L} \right) \tag{5}$$

The force - displacement relationship is

$$v(x) = \frac{\overline{f}}{E \cdot I} \cdot \left(\frac{L}{\pi} \right)^2 \cdot \left[\sin\left(\frac{\pi \cdot x}{L} \right) \right] \tag{6}$$

And the corresponding bending moments at the middle is

$$M = -\overline{f} \cdot \left(\frac{L}{\pi} \right)^2 \tag{7}$$

5. ELASTOPLASTIC BEHAVIOUR

We refer to the usual hypotheses of the plastic beam theory (Massonnet, 1962, Moy, 1996) and consider the case of shape function A. The plastic axial force and the plastic bending moment of the rectangular section $(b \times h)$ are respectively

$$N_p = b \cdot h \cdot \sigma_y \quad (M = 0) \qquad M_p = \frac{1}{4} \cdot b \cdot h^2 \cdot \sigma_y \quad (N = 0) \tag{8}$$

For any N and M, the frontier of the plastic domain is given by the equation

$$\frac{M}{M_p} = 1 - \left(\frac{N}{N_p}\right)^2 \tag{9}$$

or, by putting $\nu = N/N_p$ and $\mu = M/M_p$, by the equation:

$$\mu = 1 - \nu^2 \tag{10}$$

Table 2 list the coordinates of some points of the frontier, which will be considered in the following

Table 2 Coordinates of the frontier of the plasticization domain

$\nu = N/N_p$	$0/4$	$1/4$	$2/4$	$3/4$	$4/4$
$\mu = M/M_p$	$16/16$	$15/16$	$12/16$	$7/16$	$0/16$

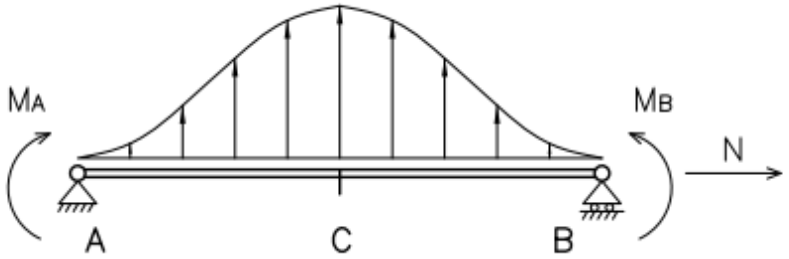

Fig. 3 Simply supported beam subjected to cosinusoidal pressure profile and to plastic moment applied at the ends

In a loading process starting from zero, we increase the load intensity $\overline{f}$. When $\overline{f}$ reaches the value

$$\overline{f}_y^I = \alpha M_{Ap} / L^2 = \left(\frac{1}{4} \cdot \frac{b \cdot h^2 \cdot \sigma_y}{L^2} \cdot \frac{24 \cdot \pi^2}{3 + \pi^2}\right) \cdot \mu \tag{11}$$

two plastic hinges at ends A and B of the beam form. The corresponding deflection and the bending moment at the middle point C are respectively

$$\mathrm{v}_C\left(x = \frac{L}{2}\right) = \frac{L^2}{E \cdot I} \cdot \frac{1}{4} \cdot b \cdot h^2 \cdot \sigma_y \cdot \frac{48 + \pi^4}{32 \cdot \pi^2 \cdot \left(3 + \pi^2\right)} \cdot \mu \tag{12}$$

$$M_C^I\left(x=\frac{L}{2}\right)=-\frac{1}{4}b\cdot h^2\cdot f_y\cdot\frac{6+\pi^2}{2\cdot\left(3+\pi^2\right)}\cdot\mu \tag{13}$$

The bending moment still available for the middle section is

$$\Delta M_C^I=M_p-M_C^I=\frac{1}{4}b\cdot h^2\cdot\sigma_y\cdot\mu\cdot\left[1-\frac{6+\pi^2}{2\cdot\left(3+\pi^2\right)}\right] \tag{14}$$

After the formation of the two plastic hinges at the ends, a further loading increase gives rise to a redistribution of the bending moment along the beam. In this phase the load deflection path can be derived with reference to a simply supported beam, subjected to the end constant moments $M_{Ap}=M_{Bp}$ and loaded by the same cosinusoidal profile (Fig. 3). Such a solution allows us to state a relationship between the increments of the load intensity and the corresponding increments of the displacements $\Delta\mathrm{v}$ and of the bending moments ΔM_C

$$\Delta\mathrm{v}(x)=\frac{\Delta\overline{f}}{E\cdot I}\cdot\left\{\frac{x^4}{48}-\frac{L^4}{32\cdot\pi^4}\cdot\left[\cos\left(\frac{2\cdot\pi\cdot x}{L}\right)\right]-\frac{L}{24}\cdot x^3-\frac{L^2}{16\cdot\pi^2}\cdot x^2+\frac{3+\pi^2}{48\cdot\pi^2}\cdot L^3\cdot x+\frac{L^4}{32\cdot\pi^4}\right\} \tag{15}$$

$$\Delta M_C=-\Delta\overline{f}\cdot L^2\cdot\left(\frac{4+\pi^2}{16\cdot\pi^2}\right) \tag{16}$$

The superposition of such increments at the end point Y of the elastic solution, allows to obtain the total displacement relationship (Fig. 4).

By equating Eq. (14) to Eq. (16)

$$\Delta M_C=\Delta M_C^I \tag{17}$$

we derive the load increment which leads to form a plastic hinge in section C

$$\Delta\overline{f}_y=\frac{1}{4}\cdot\frac{b\cdot h^2\cdot f_y}{L^2}\cdot\frac{16\cdot\pi^4}{2\cdot\left(3+\pi^2\right)\cdot\left(4+\pi^2\right)}\cdot\mu \tag{18}$$

The corresponding displacement increment is

$$\Delta\mathrm{v}_C=\frac{L^2}{E\cdot I}\cdot\frac{1}{4}\cdot b\cdot h^2\cdot f_y\cdot\frac{5\cdot\pi^4+12\cdot\pi^2+48}{48\cdot\left(3+\pi^2\right)\cdot\left(4+\pi^2\right)}\cdot\mu \tag{19}$$

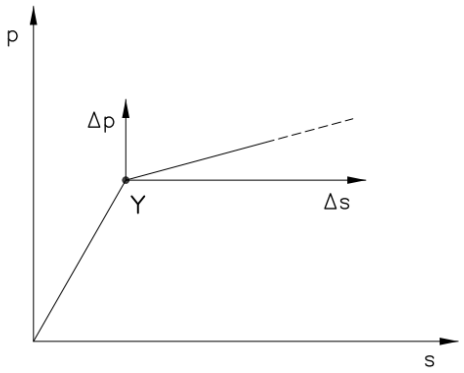

Fig. 4 Superposition of the plastic phase to the elastic one

The most relevant results for the case of shape function B are

$$M_C\left(x=\frac{L}{2}\right)=-q\cdot\left(\frac{L}{\pi}\right)^2 \tag{20}$$

$$\overline{f}_y=\frac{1}{4}\cdot b\cdot h^2\cdot f_y\cdot\left(\frac{\pi}{L}\right)^2\cdot\mu \tag{21}$$

$$\mathrm{v}_C\left(x=\frac{L}{2}\right)=\frac{1}{E\cdot I}\cdot\frac{1}{4}\cdot b\cdot h^2\cdot f_y\cdot\left(\frac{L}{\pi}\right)^2\cdot\mu \tag{22}$$

6. AN APPLICATION AND F.E. CORROBORATION

We consider a tied bar, composed by two rectangular rods having section (70x10)mm^2 and jointed by rivets placed every L= 350 mm. A yielding stress $\sigma_y=240\,N/mm^2$ has been assumed. Five levels of axial force are considered: $\left(\nu=0/4\div1/4\div2/4\div3/4\div4/4\right)$. For each ν level and for both shape functions A and B, the corresponding load displacement relationships have been computed. Results are shown in Figs. 5, 6, 7 and 8. Each graph is related to a value of $\nu=N/N_p$. The abscissas give the displacements v_C, corresponding to half opening of the gap between the rods. The ordinates quote the corresponding loading level.

Such results were corroborated by a first set of simple FEM analyses (FEM1). The four FEM1 load displacement curves have been reported in the same graphs (line c) and confirm the analytical results. Afterward a more refined FEM solution (FEM2) took into account the presence of the (ø=16mm) holes where the rods are riveted. The

presence of the holes makes the end sections weaker and more flexible with respect to the current rod characteristics. Such a reduction was modelled by grading the thickness of the elements in their end zones. Also these results were reported in the aforementioned graph (line d). As one can see, for $(\nu = 0/4 \div 1/4 \div 2/4)$ FEM2 solutions result closer to those provided adopting shape function A, while for $(\nu = 3/4)$ the curve is in between the two extreme solutions.

A synthesis of the results is given in Fig. 10. The abscissas give the displacements v_C, while the ordinates quote the value of ν corresponding to first plasticization. For the analytical solutions such a point correspond to the knees of the curves. For FEM1 and FEM2 solutions the point corresponding to a residual plastic strain of 0,2% at an edge of the section was chosen. According to this reference, FEM2 solutions result more restrictive with respect to the analytical ones.

As concern the structural capacity of the tie, from the exam of Figs. 5 ÷ 8 and 10 we deduce the following conclusions:

- the yielding of the sections is accompanied by an evident gap between the rods.
- an increase of the axial force applied to the tie gives rise to a corresponding decrease of the yielding pressure and to lower values of the gaps at yielding.
- the presence of rust swelling reduces the bearing capacity of the tie and such a reduction increases with the intensity of the axial force.

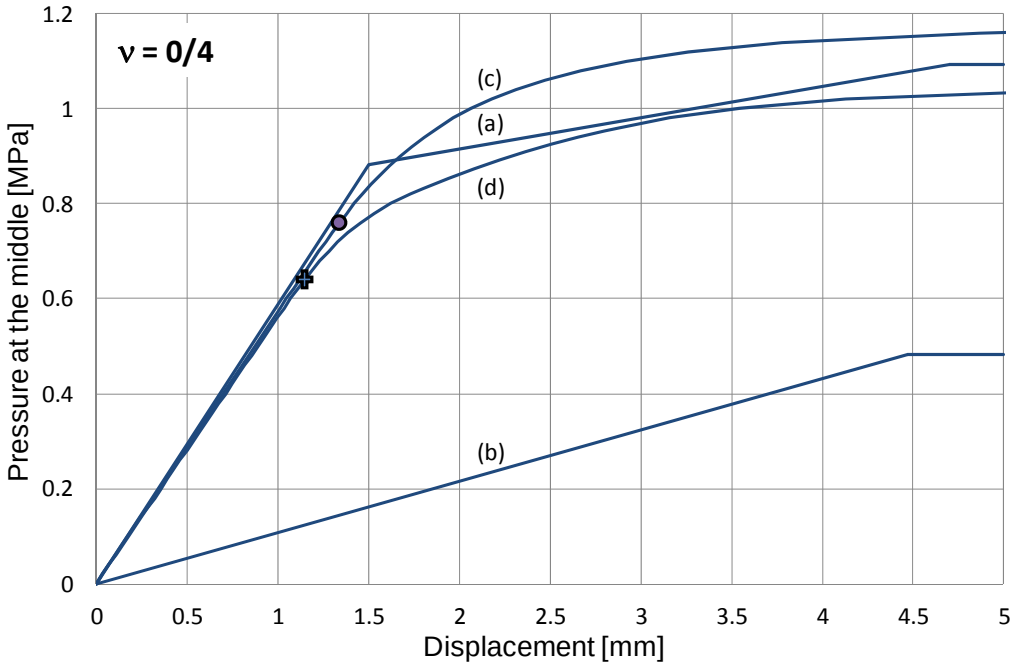

Fig. 5 Pressure displacement relationships for $\nu = 0/4$. Solutions for: (a) cosinusoidal pressure profile; (b) sinusoidal pressure profiles; (c) F.E. solution without section reduction due to the rivet hole; (d) F.E. solution with section reduction due to rivet hole

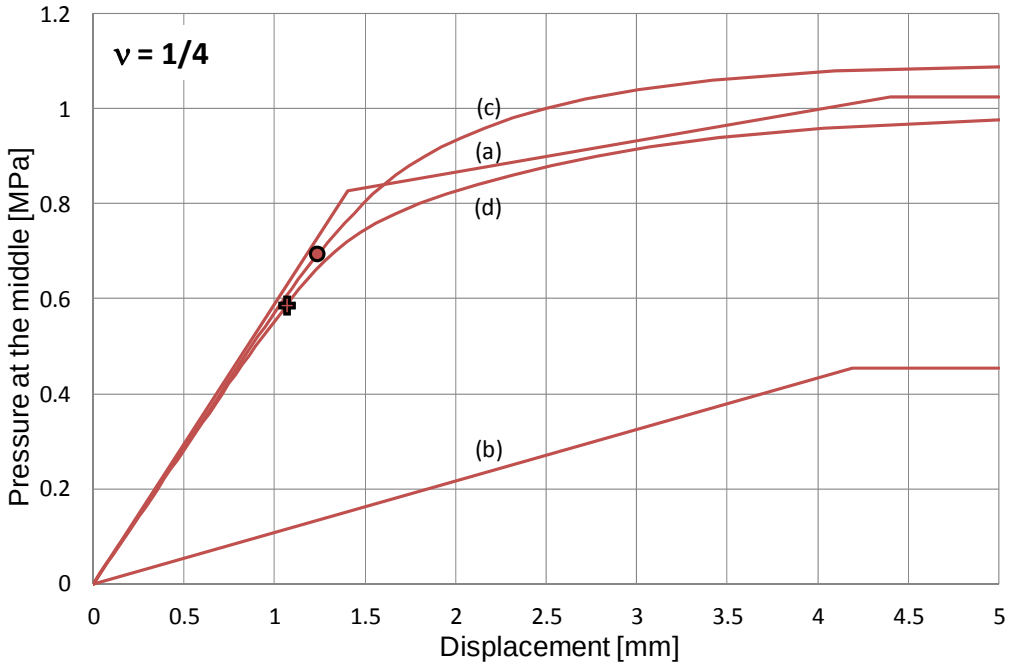

Fig. 6 Pressure displacement relationships for $\nu = 1/4$. Solutions for: (a) cosinusoidal pressure profile; (b) sinusoidal pressure profiles; (c) F.E. solution without section reduction due to the rivet hole; (d) F.E. solution with section reduction due to rivet hole

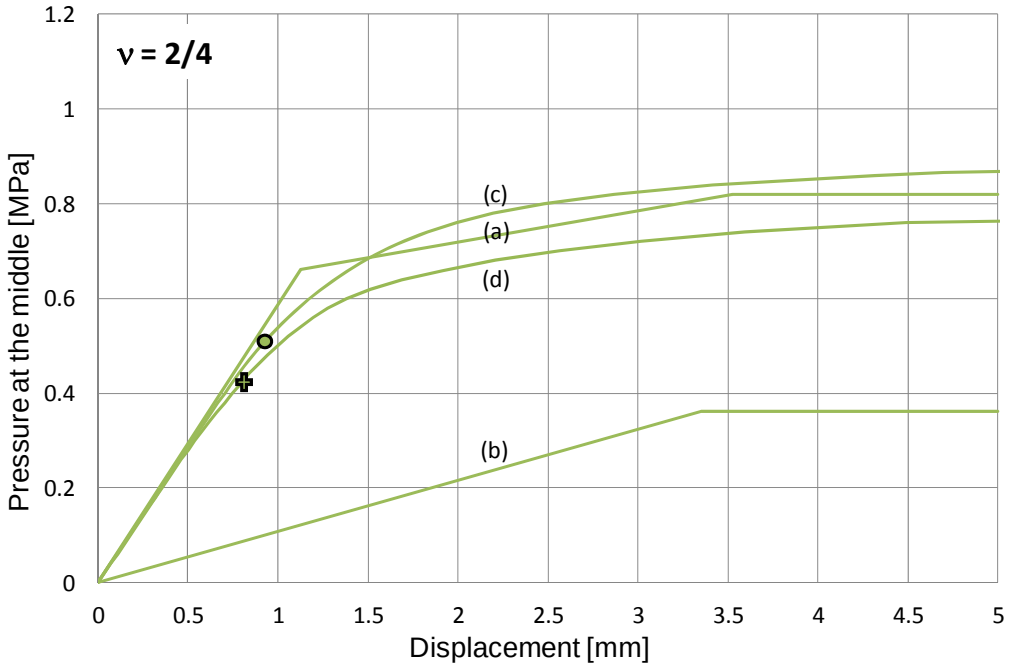

Fig. 7 Pressure displacement relationships for $\nu = 2/4$. Solutions for: (a) cosinusoidal pressure profile; (b) sinusoidal pressure profiles; (c) F.E. solution without section reduction due to the rivet hole; (d) F.E. solution with section reduction due to rivet hole

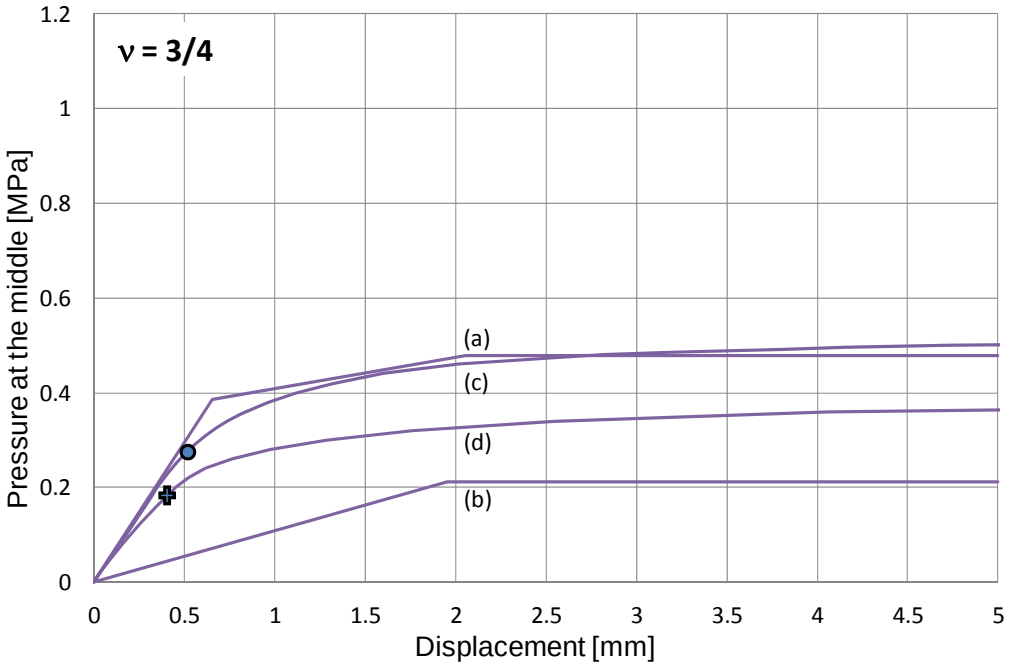

Fig. 8 Pressure displacement relationships for $\nu = 3/4$. Solutions for: (a) cosinusoidal pressure profile; (b) sinusoidal pressure profiles; (c) F.E. solution without section reduction due to the rivet hole; (d) F.E. solution with section reduction due to rivet hole

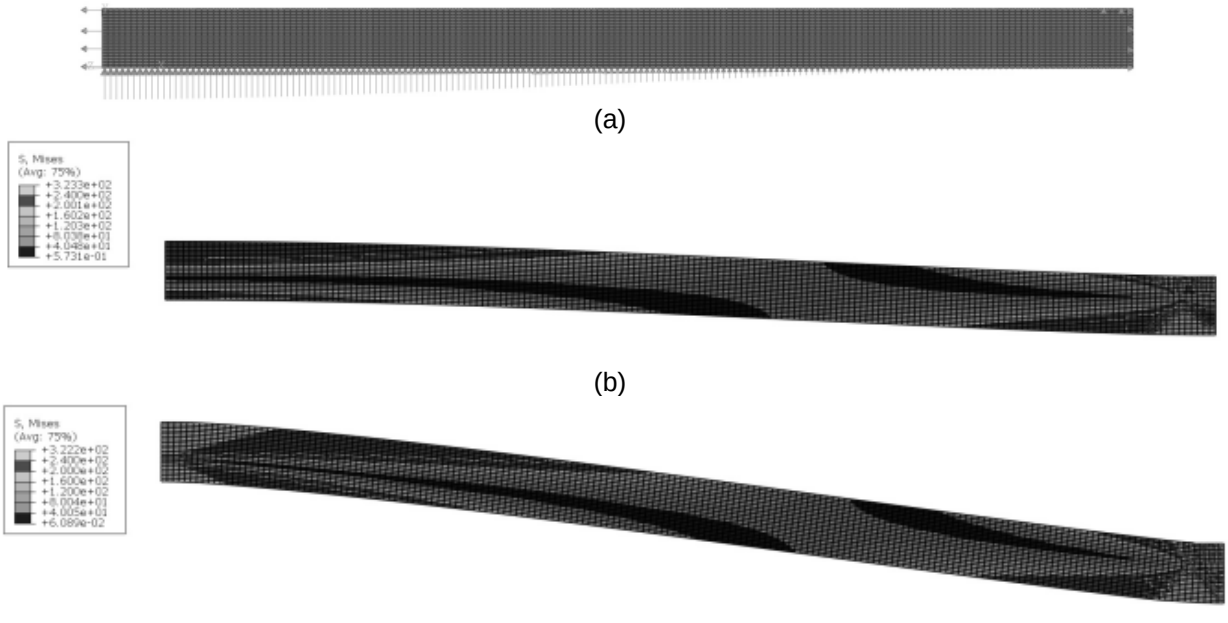

(a)

(b)

(c)

Fig. 9 ABAQUS-FEM2 comparison analyses. Axial force (v = 1/4). Mesh composed of 21 x 176 nodes and 3500 elements. (a) mesh and loads distributions; (b) deformed shape and Von Mises stresses at yielding (p = 0.82 MPa); (c) deformed shape for p = 0.96 MPa

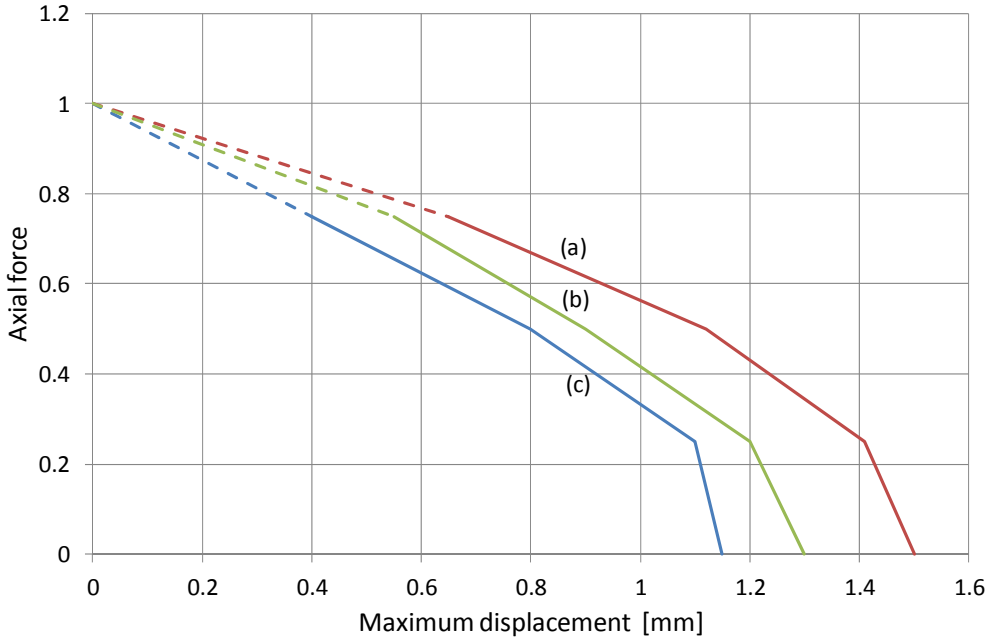

Fig. 10 Relationships between axial force and maximum displacement for: (a) cosinusoidal pressure profile; (b) F.E. solution without section reduction due to the rivets hole; (c) F.E. solution with section reduction due to rivets hole

7. CONCLUSIONS

Structural elements composed by riveted angles and sheets exhibit over time dangerous distortions, provoked by the rust grown inside the interstices and to its swelling over time.

In this paper a model suitable to study the residual bearing capacity of riveted steel ties deformed by the swelling due to the rust, has been proposed.

The results are coherent and agree with those of FEM analyses, carried out for the sake of corroboration.

Yielding of the sections is accompanied by an evident gap between the rods. The increase of the axial force applied to the tie gives rise to a corresponding decrease of the yielding pressure and to lower values of the gaps at yielding. In other words, the presence of rust swelling reduces the bearing capacity of the tie and such a reduction increases with the intensity of the axial force.

We consider such results promising and open to improvements both from the methodological and the applicative points of view in further phases of the research.

REFERENCES

Malerba, P.G. (2013), “Inspecting and repairing old bridges: experiences and lessons”, *Structure and Infrastructure Engineering*, (2013), Published online - in press DOI: 10.1080/15732479.2013.7690100.976

Massonnet, C.H. and Save, M. (1965), “Plastic Analysis and Design”, **1**, Beams and frames, Blaisdell London.

Moy, S.S.J.. (1981). “Plastic methods for steel and concrete structures”, The Macmillan Press Ltd, ISBN 0333 27563 2, ISBN 0 333 27564 0 pbk.

APPENDIX 1 LIST OF SYMBOLS

b	Width of the rod
h	Thickness of the rod
L	Pitch between the rivets
$f(x)$	Interstitial pressure function
$\overline{f}$	Maximum interstitial pressure
E	Modulus of elasticity
I	Moment of inertia of the rod
σ_y	Steel yielding stress
v	Displacement function
N	Axial force
N_p	Ultimate (plastic) axial force
M	Bending moment
M_p	Ultimate (plastic) bending moment
α, β	Numerical coefficients
$\nu = N/N_p$	Ratio between the axial force and its ultimate value
$\mu = M/M_p$	Ratio between the bending moment and its ultimate value
$\overline{f}^I_y$	Load intensity when the first plastic hinge forms
$\Delta\overline{f}^I_y$	Increment of the load intensity at the formation of the plastic hinge in C.
M^I_c	Bending moment in C when the first plastic hinges form in A and B.
ΔM^I_c	Bending moment still available at the middle when the first plastic hinges form in A and B.
$\Delta\mathrm{v}(x)$	Displacement increments in the plastic phase.